Dalton Transactions

COMMUNICATION

View Article Online
View Journal | View Issue

Cite this: *Dalton Trans.*, 2019, **48**, 9043

Received 17th April 2019,
Accepted 29th May 2019

DOI: 10.1039/c9dt01633c

rsc.li/dalton

Cation exchange reversibly switches rotor speed and is monitored by a networked fluorescent reporter†

Merve S. Özer, Indrajit Paul, Abir Goswami and Michael Schmittel *

Framework 1, a freely rotating turnstile, is transformed by sequential metal ion addition into the coordination-based double-minimum rotors $[M_2(1)]^{2n+}$ that operate at 8 kHz (M = Zn^{2+}; n = 2) and 30 kHz (M = Cu^{+}; n = 1). In a network with the fluorescent receptor 2, the metal ion exchange at $[M_2(1)]^{2n+}$ and thus indirectly the rotor speed is reported by distinct fluorescence changes at 2.

Among the many types of molecular devices,[1] thermally activated turnstiles[2] and rotors[3] allow us to study and comprehend the relationship between motion and smart molecular properties,[4] as lately demonstrated in catalytic rotary machinery.[5] The finding that product inhibition and catalytic activity directly depend on the machine speed[5] suggests that one does not need a unidirectional motor for sophisticated effects in catalysis. Such results ask for a more systematic exploration of rotor systems with speed regulation.[6]

Despite recent advances,[6] reversible toggling of rotational speed in rotors needs further exploration, in particular when the course of switching is to be reported by an optical signal. As shown by Hosseini, it is possible to control the motion of turnstiles by addition of metal ions (stop-go) and monitor the process by luminescence changes.[2a,7] For instance, in a turnstile containing a bis-pyridyl terminated rotator and a tridentate-appended stator, drastic emission changes in the open *vs.* closed state (with Ag^{+} and Pd^{2+}) allowed monitoring of the reversible ON/OFF switching of motion.[2b]

Implementation of speed regulation in rotors linked with optical monitoring requires matching of two functions in one device at the same time. Due to our expertise in networking devices[8] we considered another approach, *i.e.* to link an external optical reporter to the rotor by chemical signalling. Such protocol constitutes an adaptable toolbox that could be applied to a variety of rotor and optical reporter systems.

Here, we report on a networked system in which the two-state behaviour of rotor **1** that is reversibly regulated from slow to fast motion by addition/exchange of different metal ions is monitored by luminescence changes at a remote receptor **2** (Scheme 1). Our design was guided by the following considerations: intrinsic rotation within the framework **1** occurs about a tolane unit[9] and thus should proceed without a sizable barrier as in a typical turnstile. The situation ought to change once metal ions (Zn^{2+} or Cu^{+}) ions are added, since the pyridine terminals are expected to bind to the metal-loaded phenanthroline stations *via* HETPYP-I (HETeroleptic PYridine and Phenanthroline Metal)[10] complexation. Now the arm is expected to exchange at defined speed between the two degenerate metal-loaded stations. The luminescent aza-crown ether **2** was designed for communication with **1** as we expected different emission for the free and cation-loaded receptor.

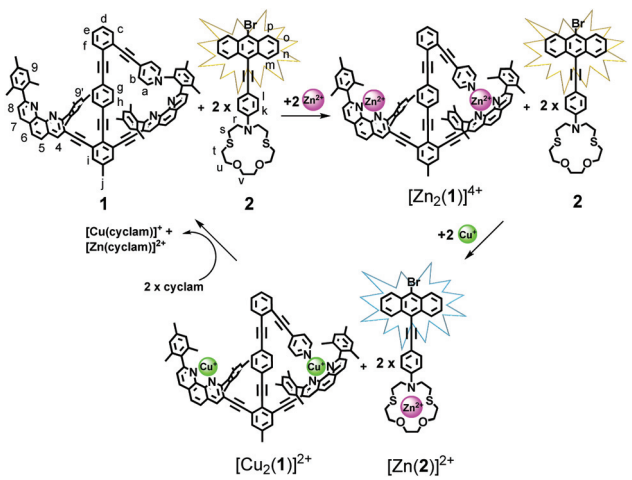

Scheme 1 Communication between nanorotor **1** and reporter **2** upon sequential addition of Zn^{2+} and Cu^{+} ions.

Center of Micro and Nanochemistry and Engineering, Organische Chemie I, Universität Siegen, Adolf-Reichwein-Str. 2, D-57068 Siegen, Germany.
E-mail: schmittel@chemie.uni-siegen.de; Tel: +49(0) 2717404356

†Electronic supplementary information (ESI) available: Experimental procedures, compound characterizations, spectral data, UV-vis titrations data. See DOI: 10.1039/c9dt01633c

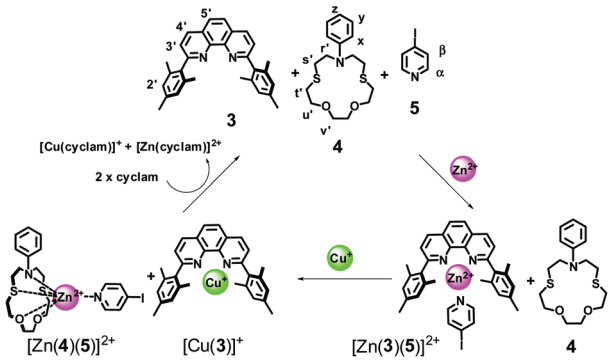

Scheme 2 Self-sorting of ligands **3**, **4** and **5** in the presence of Zn^{2+} and Cu^{+} ions.

Before addressing the precise design (Scheme 1) of the rotor and luminescence reporter, we optimized the involved binding sites by studying various two-step self-sorting events. We observed that the 1 : 1 : 1 blending of the shielded phenanthroline **3**, aza-crown ether **4** and 4-iodopyridine (**5**) in presence of one equivalent of Zn^{2+} (Scheme 2) cleanly furnished the HETPYP-I[10] complex $[Zn(\mathbf{3})(\mathbf{5})]^{2+}$. In the ^{1}H NMR, all phenanthroline protons of **3** were downfield shifted while those of pyridine, *e.g.* α-protons, were moved upfield from 8.25 to 7.78 ppm (Fig. 1a and b). The aza-crown ether **4** remained unaltered attesting a two-fold incomplete[11] self-sorting. In the second self-sorting, addition of Cu^{+} triggered a translocation of Zn^{2+} from $[Zn(\mathbf{3})(\mathbf{5})]^{2+}$ to aza-crown ether **4** to furnish $[Zn(\mathbf{4})(\mathbf{5})]^{2+}$ while copper(I) coordinated to phenanthroline **3** (85%). Importantly, as the binding of Cu^{+} to phenanthroline **3** in CH_2Cl_2 ($\log K$ = 5.42 ± 0.10, see Fig. S63†) is stronger than that of Zn^{2+} ($\log K$ = 4.58 ± 0.58, see Fig. S64†), copper(I) replaced zinc(II) at the phenanthroline binding site of **3** in

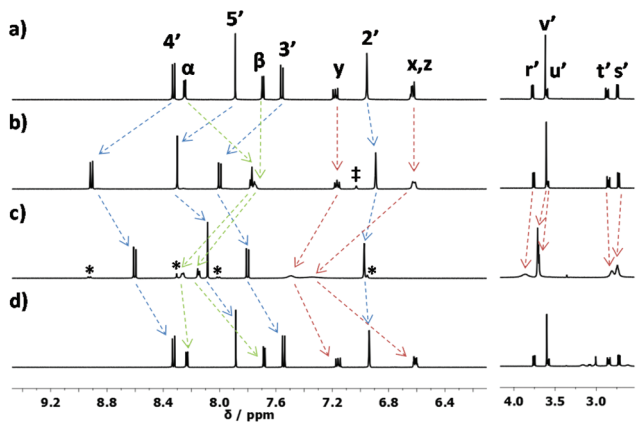

Fig. 1 Partial ^{1}H NMR (500 MHz, 25 °C) of (a) **3**, **4** and **5** (1 : 1 : 1 ratio) in CD_2Cl_2, (b) $[Zn(\mathbf{3})(\mathbf{5})]^{2+}$ and **4** in CD_2Cl_2 : CD_3CN (98 : 2) after $Zn(OTf)_2$ addition, (c) after $[Cu(CH_3CN)_4]PF_6$ addition to b: $[Zn(\mathbf{4})(\mathbf{5})]^{2+}$ and $[Cu(\mathbf{3})]^{+}$, (d) after cyclam addition to c: **3**, **4** and **5** in CD_2Cl_2 : CD_3CN (98 : 2). (‡: The corresponding signal belongs to 2′-H caused by interference of **3** with **4**; self-sorting is >98%; *: Corresponding proton signals of $[Zn(\mathbf{3})]^{2+}$ from which 15% of Zn^{2+} was not translocated).

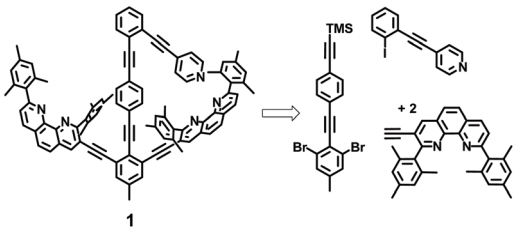

Scheme 3 Brief retrosynthetic analysis of ligand **1**.

CD_2Cl_2 : CD_3CN (98 : 2). In the ^{1}H NMR all proton signals of phenanthroline **3** were shifted upfield while both aromatic and aliphatic protons of aza-crown ether **4** showed downfield shifts as a result of zinc(II) binding (Fig. 1c). Finally, two equiv. of cyclam were added for removal of Cu^{+} and Zn^{2+} in order to regenerate the initial state represented by the free ligands **3**, **4** and **5** (see NMR, Fig. 1d).

Guided by this model study, the design of the rotor and reporter was finalized (Scheme 1). In scaffold **1** the pyridine arm and shielded phenanthroline stations are covalently connected preventing the possibility of pyridine translocation in presence of Zn^{2+} and Cu^{+} as in the model self-sorting.

Scaffold **1** was synthesized through a series of Sonogashira couplings in 15 steps and characterized by NMR, ESI-MS and elemental analysis (Scheme 3, ESI†). Characteristic signals in the ^{1}H NMR proved the formation of **1**, *e.g.* peaks of the pyridine protons α-H and β-H appeared at 8.57 and 7.44 ppm in addition to distinctive phenanthroline proton signals. The MS peak at m/z = 1270.8 showed the expected mass for $[\mathbf{1} + H]^{+}$.

For fluorescence monitoring, the aza-crown receptor in **2** was decorated with an anthracene unit. It was synthesized as described in the ESI† and characterized by spectroscopic methods and ESI-MS. After excitation at λ = 410 nm, the system **2** showed a bright yellow emission at λ = 552 nm as a result of intramolecular charge transfer (ICT). When the aza-crown ether part was coordinated to zinc(II), the fluorescence wavelength shifted to λ = 448 and 475 nm (*vide infra*).

Firstly, $[Zn_2(\mathbf{1})]^{4+}$ was prepared by mixing **1** and $Zn(OTf)_2$ in a 1 : 2 ratio. Phenanthroline protons 4-H to 8-H shifted downfield owing to zinc(II) ion coordination, while signals of pyridine protons α-H broadened and moved upfield, indicating that the zinc(II)-bound pyridine terminal was located in the shielding region of the mesityl groups of the zinc(II) phenanthroline stations (Fig. 2a and b). ESI-MS confirmed the formation by a peak at m/z = 858.0 representing $[Zn_2(\mathbf{1})(H_2O)](OTf)_2^{2+}$. Its hydrodynamic radius was calculated to 11 Å by using $D = 4.7 \times 10^{-10}$ m^2 s^{-1} from DOSY measurements (the DFT-computed theoretical radius is 9.6 Å). The single set of signals in the ^{1}H NMR suggested rapid exchange of the pyridine arm between both zinc(II)-loaded phenanthroline stations. The kinetics of motion in $[Zn_2(\mathbf{1})]^{4+}$ was determined by a VT ^{1}H NMR study from 25 °C to −75 °C in CD_2Cl_2/CD_3CN (80 : 20) (Fig. 3a); the solvent mixture[12] was required to keep the complex $[Zn_2(\mathbf{1})]^{4+}$ soluble. At 25 °C the single set of signals for the phenanthroline protons attested fast exchange,

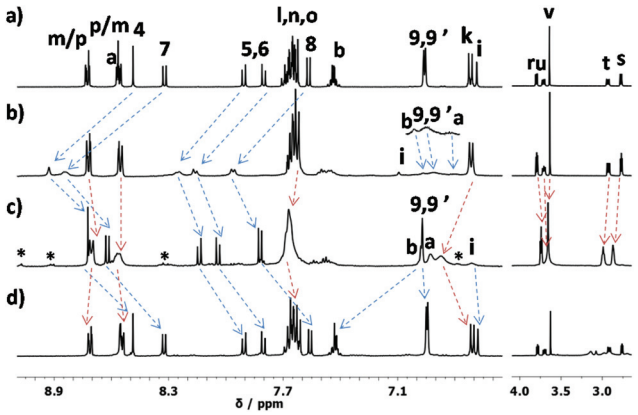

Fig. 2 Partial ^{1}H NMR (500 MHz, 25 °C) of (a) **1** and **2** (1 : 2 ratio) in CD_2Cl_2, (b) after $Zn(OTf)_2$ addition to a: $[Zn_2(\mathbf{1})]^{4+}$ and **2** in $CD_2Cl_2 : CD_3CN$ (98 : 2), (c) after $[Cu(CH_3CN)_4]PF_6$ addition to b: $[Cu_2(\mathbf{1})]^{2+}$ and $[Zn(\mathbf{2})]^{2+}$ in $CD_2Cl_2 : CD_3CN$ (98 : 2), (d) after cyclam addition to c: **1** and **2** in $CD_2Cl_2 : CD_3CN$ (98 : 2) (*: Corresponding proton signals of $[Zn_2(\mathbf{1})]^{4+}$ from which 9% of Zn^{2+} was not translocated).

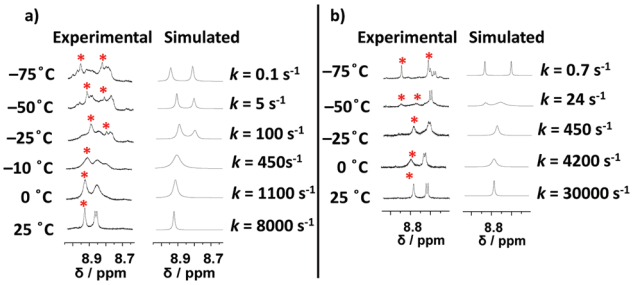

Fig. 3 Partial VT ^{1}H NMR (600 MHz) at various temperatures of (a) $[Zn_2(\mathbf{1})]^{4+}$ in $CD_2Cl_2 : CD_3CN$ (80 : 20), (b) $[Cu_2(\mathbf{1})]^{2+}$ in CD_2Cl_2.

while rotational exchange slowed down visibly at −25 °C. Now two sets of signals emerged for phenanthroline proton 4-H, one resonating at 8.92 ppm for the pyridine → Zn^{2+} complexed site and the other at 8.81 ppm for the exclusively zinc(II)-loaded phenanthroline. The exchange frequency was determined as $k_{25} = 8000\ s^{-1}$ using WinD-NMR;[13] the full set of activation data is depicted in Table 1.

Similarly, the reaction of two equiv. of $[Cu(CH_3CN)_4]PF_6$ with **1** furnished $[Cu_2(\mathbf{1})]^{2+}$ as proven by ^{1}H NMR (Fig. 2a and c). Compared to nanorotor $[Zn_2(\mathbf{1})]^{4+}$, the phenanthroline protons were shifted upfield upon Cu^+ coordination while the pyridine protons were slightly shifted downfield (Table 2). In the ESI-MS a signal at m/z = 719.5 (Fig. S58†) showed the formation of $[Cu_2(\mathbf{1})(CH_3CN)]^{2+}$. The diffusion coefficient $D = 4.4 \times 10^{-10}\ m^2\ s^{-1}$ (DOSY) suggested a hydrodynamic radius of 12 Å (compare to 9.6 Å from the DFT-computed structure). As before, the ^{1}H NMR showed fast exchange of the pyridine arm between both copper(I)-loaded phenanthroline stations. In the VT ^{1}H NMR performed in CD_2Cl_2 from +25 to −75 °C (Fig. 3b), a splitting of protons 4-, 5-, 6-, 7-, 8-, 9- and 9′-H was observed. Kinetic parameters were calculated from the changes of proton 4-H in **1**, which split into copper(I)-loaded (8.74 ppm) and pyridine → Cu^+ complexed (8.85 ppm) phenanthroline stations at −50 °C. The exchange rate at room temperature was determined to $k_{25} = 30\,000\ s^{-1}$ (Table 1).

Table 1 Experimental activation parameters of nanorotors and rotational frequency at 25 °C

Nano-rotors	$\Delta H^{\ddagger}$ (kJ mol^{-1})	$\Delta S^{\ddagger}$ (J mol^{-1} K^{-1})	$\Delta G^{\ddagger}$ (kJ mol^{-1})	k_{25} (s^{-1})
$[Zn_2(\mathbf{1})]^{4+}$	53.4 ± 0.4	9.7 ± 2.0	50.5	8000
$[Cu_2(\mathbf{1})]^{2+}$	50.4 ± 0.3	9.9 ± 1.2	47.4	30 000

Table 2 ^{1}H NMR shift comparison of some characteristic protons of ligand **1**, $[Zn_2(\mathbf{1})]^{4+}$ and $[Cu_2(\mathbf{1})]^{2+}$ (ligand **1** and $[Cu_2(\mathbf{1})]^{2+}$ were measured in CD_2Cl_2 and $[Zn_2(\mathbf{1})]^{4+}$ was measured in $CD_2Cl_2 : CD_3CN$ (96 : 4))

Protons	δ/ppm ligand **1**	δ/ppm $[Zn_2(\mathbf{1})]^{4+}$	δ/ppm $[Cu_2(\mathbf{1})]^{2+}$
a-H	8.57	6.56	6.67
b-H	7.44	7.01	7.10
4-H	8.49	8.94	8.77
5 and 6-H	7.91, 7.80	8.27, 8.17	8.13, 8.06
7-H	8.32	8.87	8.66
8-H	7.57	7.97	7.90
9 and 9′-H	6.97, 6.96	6.94	6.96

The stochastic rotational exchange in nanorotors $[Zn_2(\mathbf{1})]^{4+}$ and $[Cu_2(\mathbf{1})]^{2+}$ occurs at activation barriers $\Delta G^{\ddagger}_{25}$ of 50.5 and 47.4 kJ mol^{-1}, respectively. Since, departure of the rotator arm is endergonic and rate determining[3a] it was expected that rotor $[Cu_2(\mathbf{1})]^{2+}$ has a slightly higher rotational rate than $[Zn_2(\mathbf{1})]^{4+}$ because the pyridine → copper(I) (18.3 kJ mol^{-1})[3e] is less endergonic than the pyridine → zinc(II) dissociation (22.2 kJ mol^{-1}; Fig. S65†). Moreover, dissociation of pyridine from the metal center may be accelerated *via* an S_N2 displacement by nucleophilic components in the solvent, *e.g.* acetonitrile.[12]

To probe the interdependent system of rotor and fluorescence reporter, ligands **1** and **2** were mixed (1 : 2). The UV-vis analysis in 0.2% CH_3CN in CH_2Cl_2 displayed absorptions at λ = 255, 438 and 458 nm, characteristic of receptor **2** (Fig. 4a). After addition of two equiv. of $Zn(OTf)_2$, nanorotor $[Zn_2(\mathbf{1})]^{4+}$ was afforded while receptor **2** remained unloaded, as suggested in NMR (Fig. 2b) and also by UV-vis and emission spectra. The UV-vis spectrum still displayed the absorption bands of the free receptor **2** at λ = 255, 438 and 458 nm (Fig. 4a and b). Equally, the emission profile did not change after addition of zinc(II); the maximum remained at λ = 552 nm as in the case of receptor **2** only (Fig. 4c and d). It is important to note that the zinc(II) rotor does not exhibit any emission when excited at λ = 410 nm.

To test the communication *via* metal translocation, two equiv. of $[Cu(CH_3CN)]PF_6$ were added. ^{1}H NMR results suggested that 91% of the copper(I) rotor $[Cu_2(\mathbf{1})]^{2+}$ formed while parallel Zn^{2+} was translocated to receptor **2** (Fig. 2c). The NMR signals of **2** changed on the way to $[Zn(\mathbf{2})]^{2+}$, *e.g.* proton k-H shifted downfield from 6.71 to 6.87 ppm. At the same time, the UV-vis analysis equally validated that Zn^{2+} had translocated to receptor **2** to afford $[Zn(\mathbf{2})]^{2+}$ (Fig. 4b), because absorption bands

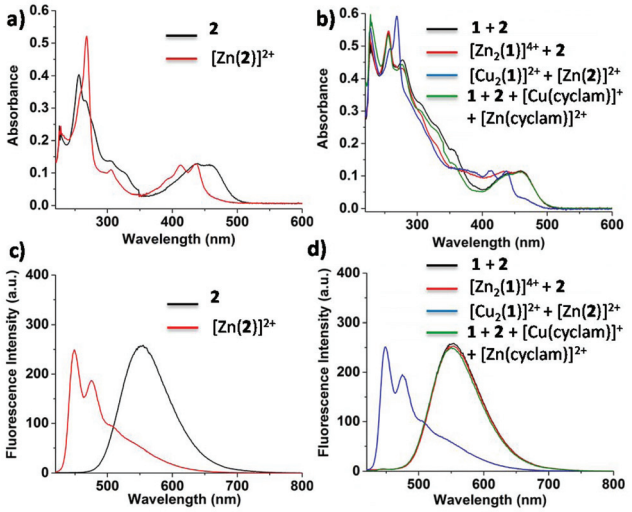

Fig. 4 Comparison of UV-vis spectra (25 °C, 0.2% CH_3CN in CH_2Cl_2) of (a) **2** and $[Zn(\mathbf{2})]^{2+}$ at 5.00 μM, (b) **1** (2.50 μM) + **2** (5.00 μM), $[Zn_2(\mathbf{1})]^{4+}$ + **2**, $[Cu_2(\mathbf{1})]^{2+}$ + $[Zn(\mathbf{2})]^{2+}$ and **1** + **2** + $[Cu(cyclam)]^{+}$ + $[Zn(cyclam)]^{2+}$; comparison of emission spectra (25 °C, λ_{exc} = 410 nm, 0.2% CH_3CN in CH_2Cl_2) of (c) **2** and $[Zn(\mathbf{2})]^{2+}$ at 1.25 μM, (d) **1** (0.625 μM) + **2** (1.25 μM), $[Zn_2(\mathbf{1})]^{4+}$ + **2**, $[Cu_2(\mathbf{1})]^{2+}$ + $[Zn(\mathbf{2})]^{2+}$ and **1** + **2** + $[Cu(cyclam)]^{+}$ + $[Zn(cyclam)]^{2+}$.

appeared at λ = 268, 412 and 438 nm, identical to the absorptions of separately prepared $[Zn(\mathbf{2})]^{2+}$. Parallel, emission spectroscopy exhibited a blue-shifted fluorescence at λ = 448 and 475 nm (Fig. 4d). Finally, four equivalents of cyclam were added to capture all copper(I) and zinc(II) ions and to resume the initial state (Fig. 2d). The process of sequential addition of metal ions (Zn^{2+} and Cu^{+}) and of cyclam was repeated up to two cycles (ESI) proving full reversibility of the networking by ^{1}H NMR and emission data.

Upon addition of two equiv. of $[Cu(CH_3CN)_4]PF_6$ with respect to rotor $[Zn_2(\mathbf{1})]^{4+}$ (3.60 μM) in the presence of receptor **2** (7.20 μM), translocation of Zn^{2+} from ligand **1** to receptor **2** took approximately 60 min in 0.2% CH_3CN in CH_2Cl_2 by UV-Vis. Due to an intermittent absorbance at 268 nm, attributed to $[Cu(\mathbf{2})]^{+}$, the mechanism is suggested as follows: first, the copper(I) ion coordinates to aza-crown **2**, then the copper(I) and zinc(II) ions slowly exchange their binding sites due to global thermodynamics since the coordination of Cu^{+} to the phenanthroline ligand ($\log K$ = 5.42) is stronger than that of Zn^{2+} ($\log K$ = 4.58) while both ions have almost identical binding data to **2** ($\log K$ = 4.08 *vs.* 3.91). Kinetic analysis suggests a first-order kinetics ($t_{1/2}$ = 762 s at 25 °C) for translocation.

The nicely agreeing emission signals of the black and green emission traces in Fig. 4d demonstrate the full reversibility of the system when it is reset by addition of cyclam.

Conclusion

In conclusion, we prepared the covalent turnstile **1** with two phenanthroline stations in the stator part and a pyridine arm as rotator, whose rotational barrier at room temperature is estimated as 2.4–2.7 kJ mol^{-1}.[9] Nanorotor $[Zn_2(\mathbf{1})]^{4+}$, formed upon addition of Zn^{2+}, operates at k_{25} = 8000 Hz and the Cu^{+}-loaded system $[Cu_2(\mathbf{1})]^{2+}$ rotates at k_{25} = 30 000 Hz. The three-step transformation of **1** (>10^9 kHz) → $[Zn_2(\mathbf{1})]^{4+}$ (8 kHz) → $[Cu_2(\mathbf{1})]^{2+}$ (30 kHz) was achieved by the sequential addition of zinc(II) and copper(I) ions with the last transformation being monitored by **2** as fluorescence reporter. While the ensemble of rotor $[Zn_2(\mathbf{1})]^{4+}$ and free receptor **2** exhibited an emission at 552 nm, the addition of copper(I) triggering zinc(II) translocation ($t_{1/2}$ = 762 s) to afford receptor $[Zn(\mathbf{2})]^{2+}$ shifted the emission to λ = 448 and 475 nm. Fully reversible ion exchange between **1** and receptor **2** was demonstrated over two cycles, indicating that multifunctional (*i.e.* rotation & emission) and multicomponent systems work in a reliable and coherent manner.

Conflicts of interest

There are no conflicts to declare.

Acknowledgements

We acknowledge generous financial support from the Deutsche Forschungsgemeinschaft (DFG Schm 647/20-2).

Notes and references

1 (*a*) J. M. Abendroth, O. S. Bushuyev, P. S. Weiss and C. J. Barrett, *ACS Nano*, 2015, **9**, 7746–7768; (*b*) S. Erbas-Cakmak, D. A. Leigh, C. T. McTernan and A. L. Nussbaumer, *Chem. Rev.*, 2015, **115**, 10081–10206.

2 (*a*) B. Godde, D. Ritaine, A. Jouaiti, M. Mauro and M. W. Hosseini, *New J. Chem.*, 2018, **42**, 7810–7815; (*b*) B. Godde, A. Jouaiti, A. Fluck, N. Kyritsakas, M. Mauro and M. W. Hosseini, *Dalton Trans.*, 2017, **46**, 14897–14906; (*c*) G. Wang, H. Xiao, J. He, J. Xiang, Y. Wang, X. Chen, Y. Che and H. Jiang, *J. Org. Chem.*, 2016, **81**, 3364–3371; (*d*) Z. Zhou, X. Zhang, Q. Liu, Z. Yan, C. Lv and G. Long, *Inorg. Chem.*, 2013, **52**, 10258–10263.

3 (*a*) P. K. Biswas, S. Saha, Y. Nanaji, A. Rana and M. Schmittel, *Inorg. Chem.*, 2017, **56**, 6662–6670; (*b*) A. Goswami, I. Paul and M. Schmittel, *Chem. Commun.*, 2017, **53**, 5186–5189; (*c*) M. Nakamura, K. Kishimoto, Y. Kobori, T. Abe, K. Yoza and K. Kobayashi, *J. Am. Chem. Soc.*, 2016, **138**, 12564–12577; (*d*) M. Krick, J. Holstein, C. Würtele and G. H. Clever, *Chem. Commun.*, 2016, **52**, 10411–10414; (*e*) S. K. Samanta and M. Schmittel, *J. Am. Chem. Soc.*, 2013, **135**, 18794–18797; (*f*) B. E. Dial, P. J. Pellechia, M. D. Smith and K. D. Shimizu, *J. Am. Chem. Soc.*, 2012, **134**, 3675–3678; (*g*) S. Hiraoka, Y. Hisanaga, M. Shiro and M. Shionoya, *Angew. Chem., Int. Ed.*, 2010, **49**, 1669–1673.

4 J. Michl and E. C. H. Sykes, *ACS Nano*, 2009, **3**, 1042–1048.

5 P. K. Biswas, S. Saha, T. Paululat and M. Schmittel, *J. Am. Chem. Soc.*, 2018, **140**, 9038–9041.

6 (*a*) Y. Wu, G. Wang, Q. Li, J. Xiang, H. Jiang and Y. Wang, *Nat. Commun.*, 2018, **9**, 1953; (*b*) G. T. Rushton, E. C. Vik, W. G. Burns, R. D. Rasberry and K. D. Shimizu, *Chem. Commun.*, 2017, **53**, 12469–12472; (*c*) A. Faulkner, T. van Leeuwen, B. L. Feringa and S. J. Wezenberg, *J. Am. Chem. Soc.*, 2016, **138**, 13597–13603; (*d*) Y. Suzuki, M. Kageyama, R. Morisawa, Y. Dobashi, H. Hasegawa, S. Yokojima and O. Kitagawa, *Chem. Commun.*, 2015, **51**, 11229–11232.

7 N. Zigon, P. Larpent, A. Jouaiti, N. Kyritsakas and M. W. Hosseini, *Dalton Trans.*, 2014, **43**, 15779–15784.

8 (*a*) M. Schmittel, *Dalton Trans.*, 2018, **47**, 6654–6659; (*b*) A. Goswami, S. Pramanik and M. Schmittel, *Chem. Commun.*, 2018, **54**, 3955–3958; (*c*) N. Mittal, S. Pramanik, I. Paul, S. De and M. Schmittel, *J. Am. Chem. Soc.*, 2017, **139**, 4270–4273.

9 (*a*) N. M. Albu, E. Bergin and D. J. Yaron, *J. Phys. Chem. A*, 2009, **113**, 7090–7096; (*b*) S. J. Greaves, E. L. Flynn, E. L. Futcher, E. Wrede, D. P. Lydon, P. J. Low, S. R. Rutter and A. Beeby, *J. Phys. Chem. A*, 2006, **110**, 2114–2121.

10 (*a*) M. Schmittel, B. He, J. Fan, J. W. Bats, M. Engeser, M. Schlosser and H.-J. Deiseroth, *Inorg. Chem.*, 2009, **48**, 8192–8200; (*b*) S. Neogi, G. Schnakenburg, Y. Lorenz, M. Engeser and M. Schmittel, *Inorg. Chem.*, 2012, **51**, 10832–10841.

11 M. L. Saha and M. Schmittel, *Org. Biomol. Chem.*, 2012, **10**, 4651–4684.

12 S. Saha, P. K. Biswas and M. Schmittel, *Inorg. Chem.*, 2019, **58**, 3466–3472.

13 H. J. Reich, *NMR Spectrum Calculations: WinDNMR, Version 7.1*, Department of Chemistry, University of Wisconsin.